ACTA ACUSTICA UNITED WITH ACUSTICA
Vol. 91 (2005) 567 – 577

Dependence of Sound Amplification on Temperature Distribution in Annular Thermoacoustic Engines

G. Penelet[1], S. Job[1], V. Gusev[1,2], P. Lotton[1], M. Bruneau[1]
[1]: Laboratoire d'Acoustique, Université du Maine, Avenue Olivier Messiaen, 72085 Le Mans Cedex 9, France
[2]: Laboratoire de Physique de l'Etat Condensé, Université du Maine, Avenue Olivier Messiaen, 72085 Le Mans Cedex 9, France

Summary
The aim of this paper is to study the influence of the shape of the temperature distribution on the thermoacoustic amplification in an annular thermoacoustic prime mover. An analytical model is presented and the acoustic field in the whole device is computed for an arbitrary temperature distribution. The obtained results demonstrate dependence of the thermoacoustic amplification not only on the maximum temperature difference but also significantly on the details of the spatial temperature distribution, which influence the structure of the acoustic field throughout the thermoacoustic core. These results provide the opportunity to predict qualitatively the variation of the thermoacoustic amplification, when the temperature distribution is modified by acoustic streaming or acoustically enhanced thermal conductivity. It may be of primary importance when trying to explain the complicated, experimentally observed dynamics of the transient process of acoustic wave amplification and saturation.

PACS no. 43.35.Ud, 43.25.Nm, 43.25+y

1. Introduction

The basic elements of a thermoacoustic prime mover are a resonant acoustic tube (filled with a gas) and a stack of solid plates subjected to a strong temperature gradient. When the temperature gradient along the stack exceeds some critical value, the thermoacoustic interaction between the fluid and the stack results in the self excitation of a high amplitude acoustic wave. Recently, thermoacoustic devices using a travelling wave phasing have been investigated and have already demonstrated high efficiency [1, 2], compared to classical standing wave devices. At the present time, there is a growing interest in improving the understanding and in optimizing the efficiency of travelling wave thermoacoustic prime movers, in order to make use of them, for instance as a mechanical source for cryocoolers. One of those devices, called the annular thermoacoustic prime mover, involves placing the stack in a closed loop resonator (as illustrated in Figure 1a), thus allowing the generation of travelling acoustic waves [3]. In such a device, the saturation of the thermoacoustic instability leading to the stationary regime is linked not only to classical nonlinear phenomena such as the cascade process of higher harmonic generation and minor losses, but also to nonlinear processes influencing the temperature distribution in the inhomogeneously heated parts of the system such as acoustically enhanced thermal conductivity (equivalent to heat transport induced by gas oscillations [4]) and the excitation of unidirectional acoustic streaming [5]. Such kinds of nonlinear interactions between the acoustic and temperature fields may firstly reduce the mean temperature gradient across the stack (with subsequent saturation of the acoustic wave amplitude), but may also change the shape of the temperature distribution, as illustrated in Figures 1b,c. While various analytical models describe classical nonlinear phenomena [6, 7, 8, 9, 10] and streaming generation [5, 11, 12], the influence of temperature distribution profile in the inhomogeneously heated parts of the device on thermoacoustic amplification is less understood. In fact, to our knowledge, the existing models neither allow to describe precisely the acoustically induced evolution of the temperature distribution during the transient regime of the prime mover operation, nor give an idea of the reverse influence of the temperature distribution on the structure of the acoustic field and on the thermoacoustic amplification process. The existing analytical models frequently consider a mean temperature gradient along the stack and do not allow for the temperature field to be other than linear in coordinate, whereas for instance forced thermal convection (due to acoustic streaming) could give to this temperature field a nonlinear shape (Figure 1b). Now, various experimental observations indicate that nonlinear effects influencing the temperature field probably play a major role [13, 14, 15]. Particularly, we expect those nonlinear effects

Received 28 May 2004,
accepted 20 January 2005.

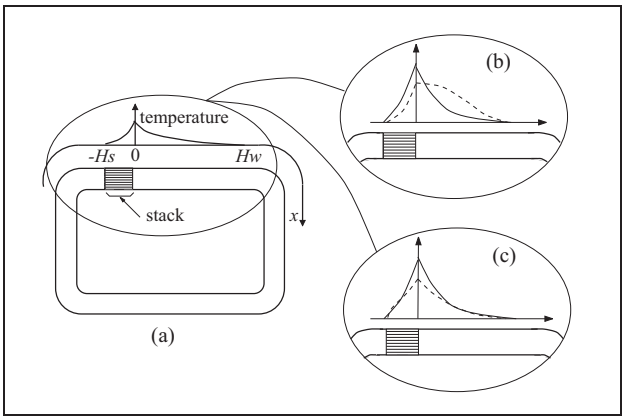

Figure 1. (a) Schematic representation of the annular thermoacoustic prime mover. (b) Qualitative representation of the acoustically induced variations of the temperature distribution (dashed line) due to acoustic streaming directed from left to right. (c) Qualitative representation of the acoustically induced variations of the temperature distribution (dashed line) due to acoustically enhanced thermal conductivity.

to be responsible for what we called the double-threshold phenomenon [15] and other complicated dynamical behaviours observed under some heating conditions in the transient regime.

A quantitative and exhaustive description of the thermoacoustic amplification process requires a numerical resolution of the equations of motion [16], but many expensive diagnostics may be wasted trying to understand the independent influence of each one of the nonlinear phenomena that control the saturation. We believe that a complementary approach would be to find the simplest description that qualitatively captures the dynamics which are typically observed in experiments. Obviously, thermoacoustic amplification and saturation processes depend on numerous parameters, but if we succeed in determining the most relevant ones that provide qualitative description, we will expect additional terms to have only quantitative effects. As pointed out before, the main deficiency we must clear up before trying to compute the transient regime is the analysis of how and why the shape of the spatial temperature distribution (i.e. linear or not) throughout the thermoacoustic core of an annular thermoacoustic prime mover has an influence on the sound amplification process. This will be the topic of the present paper.

In section 2, an analytical model for an annular thermoacoustic prime mover is presented [17]. This model, which is based on mathematical approach developed for standing wave devices [8], uses the scattering matrix formalism to describe the acoustic field in this closed loop device. There are neither restrictions on the stack length nor on the shape of the temperature field. Analytical expressions for the threshold condition and for the corresponding oscillation frequency are provided, and calculated numerically. The acoustic field in the whole device, and the total work flow are also calculated. In section 3, the role of the temperature distribution in the stack and in the inhomogeneously heated part of the resonator is investigated, from the quasi-adiabatic regime to the quasi-isothermal regime. The main result is that the temperature distribution in the resonator has a great influence on the amplification process, mainly because it significantly modifies the acoustic pressure, velocity and phase shift between them. Consequently, accounting for the effect of acoustic streaming and acoustically induced thermal conductivity in a theory describing transient interaction of the acoustic and thermal fields in the transient regime may allow to reproduce, at least qualitatively, the experimentally observed dynamics of the prime mover operation.

2. Analytical model

The device is schematically presented in Figure 1. It consists of an annular cylindrical waveguide (inner radius D_W) of length L, that can be divided into three parts, i.e. the stack ($-H_S \leq x \leq 0$), the inhomogeneously heated part of the resonator ($0 \leq x \leq H_W$), and the cold part ($H_W \leq x \leq L - H_S$). The interval $-H_S \leq x \leq H_W$ is called the thermoacoustic core. The stack is a porous material (longitudinal porosity $= 0.81$) with many cylindrical channels of inner radius D_S . Notice that in the corresponding experimental device [13, 15] the stack is made of many square channels, but the cylindrical geometry is chosen because computation times are significantly shorter. No restriction is made on the stack length H_S and on the shape of the temperature distribution in the thermoacoustic core. In our model [17], the coupling between the thermoacoustic core and the rest of the resonator is described using the scattering matrix of the thermoacoustic core, for an arbitrary temperature distribution profile $T(x)$.

2.1. Scattering matrix of the thermoacoustic core

Acoustic variables are expressed in the frequency domain, ω denoting the angular frequency. In the interval $H_W \leq x \leq L - H_S$ with homogeneous temperature distribution, the acoustic pressure $\tilde{p}(x,\omega) \equiv \tilde{p}(x)$ can be separated into its two counterpropagative components $\tilde{p}(x) = \tilde{p}^+(x) + \tilde{p}^-(x)$, where $\tilde{p}^+$ and $\tilde{p}^-$ represent the complex amplitudes of the pressure waves which propagate respectively in the $+x$ and $-x$ directions ($p(x,t) = \Re e\left(\tilde{p}(x)\mathrm{e}^{-\mathrm{i}\omega t}\right)$). In order to take into account the causality of incident, reflected and transmitted waves at the edges of the thermoacoustic core, a discrete time scale is introduced using the subscript m corresponding to the mth passing of the wave through the thermoacoustic core. Consequently, as illustrated in Figure 2, the acoustic pressure at the mth iteration can be expressed as a function of its value at the $(m-1)$th iteration and of the reflexion/transmission characteristics of the thermoacoustic core, using the scattering matrix as follows:

$$\begin{pmatrix} \tilde{p}_m^+(H_W) \\ \tilde{p}_m^-(-H_S) \end{pmatrix} = \begin{pmatrix} \mathcal{T}^+ & \mathcal{R}^- \\ \mathcal{R}^+ & \mathcal{T}^- \end{pmatrix} \begin{pmatrix} \tilde{p}_{m-1}^+(-H_S) \\ \tilde{p}_{m-1}^-(H_W) \end{pmatrix}. \quad (1)$$

In equation (2), the coefficients $\mathcal{T}^\pm$ and $\mathcal{R}^\pm$ represent the transmission and reflexion coefficients of the thermoacoustic core. To compute these coefficients, it is necessary

to solve the well-known differential equation of thermoacoustics [18] (second order differential equation with variable coefficients)

$$\frac{\mathrm{d}}{\mathrm{d}x}\left[(1-f_\nu)\frac{\mathrm{d}\tilde{p}}{\mathrm{d}x}\right]+\beta\left[1-f_\nu+\frac{f_\nu-f_\kappa}{(1-\sigma)(1+\epsilon)}\right]\frac{\mathrm{d}T}{\mathrm{d}x}\frac{\mathrm{d}\tilde{p}}{\mathrm{d}x} + \left(\frac{\omega}{a_c}\right)^2\left[1+\frac{(\gamma-1)f_\kappa}{1+\epsilon}\right]\tilde{p}=0. \quad (2)$$

Here, $T(x)$ is the mean temperature (i.e. the temperature averaged over a period of acoustic oscillations), ω is the angular frequency, a_c is the speed of sound, β is the isobaric thermal expansion coefficient, γ is the specific heat ratio of fluid, and σ is the Prandtl number. The frequency (and temperature) dependant functions f_ν and f_κ characterize the efficiciency of the viscous and thermal coupling of the acoustic field with the walls of the channel (stack channel, or waveguide). For the case of a cylindrical channel of inner radius D, these functions are

$$f_{\nu,\kappa} = \frac{2}{\mathrm{i}Y_{\nu,\kappa}}\frac{J_1(\mathrm{i}Y_{\nu,\kappa})}{J_0(\mathrm{i}Y_{\nu,\kappa})}, \quad (3)$$

$$\text{where}\quad Y_{\nu,\kappa} = (1+\mathrm{i})\frac{D}{\delta_{\nu,\kappa}}. \quad (4)$$

$\delta_\kappa = \sqrt{2\kappa(T(x))/\omega}$ is the acoustic thermal boundary layer thickness in fluid and $\delta_\nu = \sqrt{2\nu(T(x))/\omega}$ is the acoustic viscous boundary layer thickness in fluid (ν and κ denoting the temperature dependant kinematic viscosity and thermal diffusivity of the fluid). The coefficient ϵ, proportional to the ratio ϵ_f/ϵ_S of thermal effusivities of fluid and solid, characterizes heat transport in the direction normal to the direction of acoustic wave propagation. Assuming $\epsilon \ll 1$ (in fact, considering $\epsilon = 0$) and $\beta = 1/T$ (i.e. considering that the fluid is an ideal gas), equation (2) reduces to

$$\frac{\mathrm{d}^2\tilde{p}}{\mathrm{d}x^2}+\left[1+\frac{1}{1-f_\nu}\left(\frac{f_\nu-f_\kappa}{1-\sigma}-T_N(x)\frac{\mathrm{d}f_\nu}{\mathrm{d}T_N}\right)\right]\cdot\frac{1}{T_N}\frac{\mathrm{d}T_N}{\mathrm{d}x}\frac{\mathrm{d}\tilde{p}}{\mathrm{d}x} + \left(\frac{\omega}{a_c}\right)^2\frac{1}{T_N}\left[1+\frac{1}{1-f_\nu}(f_\nu+(\gamma-1)f_\kappa)\right]\tilde{p}=0, \quad (5)$$

where $T_N(x) = T(x)/T_C$, with T_C denoting the cold temperature (i.e. the temperature at the cold end of the stack). It has been demonstrated in an earlier paper dealing with standing wave prime movers [8] that transformation of this equation into an equivalent Volterra integral equation of the second kind leads to an exact solution in the form of an infinite iterative sequence of integral operators. Here, we take advantage of this result, taking into account the specific boundary conditions linked to the annular geometry of the present device. The following quantities

$$\frac{\mathrm{d}\phi_1}{\mathrm{d}x}=\left[1+\frac{1}{1-f_\nu}\left(\frac{f_\nu-f_\kappa}{1-\sigma}-T_N(x)\frac{\mathrm{d}f_\nu}{\mathrm{d}T_N}\right)\right]\cdot\frac{1}{T_N}\frac{\mathrm{d}T_N}{\mathrm{d}x}, \quad (6)$$

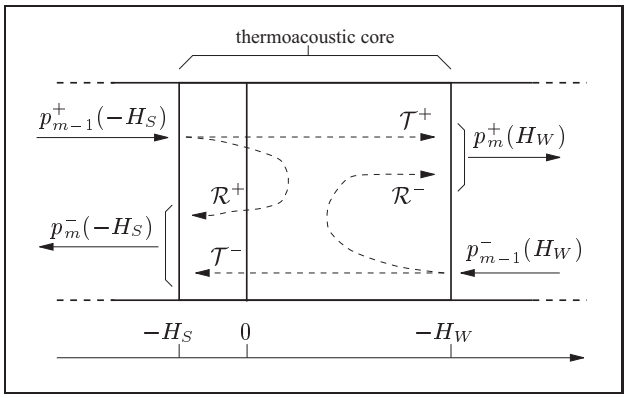

Figure 2. Reflected and transmitted waves at the edges of the thermoacoustic core.

$$\phi_0 = \frac{1}{T_N}\left[1+\frac{1}{1-f_\nu}(f_\nu+(\gamma-1)f_\kappa)\right] \quad (7)$$

are introduced, and a new spatial coordinate ξ is defined:

$$\frac{\mathrm{d}\xi}{\mathrm{d}x} = \xi_x = \mathrm{e}^{(\phi_1(x_0)-\phi_1(x))}, \quad (8)$$

where x_0 is an arbitrary origin in the reference frame. Then, defining the function

$$F(\xi) = \phi_0(x(\xi))\xi_x^{-2}, \quad (9)$$

equation (5) reduces to

$$\frac{\mathrm{d}^2\tilde{p}}{\mathrm{d}\xi^2}+k_c^2F(\xi)\tilde{p}=0, \quad (10)$$

with $k_c = \omega/a_c$. The main advantage of this formulation is that the solution can be found using an iterative method. For this purpose, equation (10) is modified into the equivalent form

$$\tilde{p}(\xi) = \tilde{p}(\xi_0)+\int_{\xi_0}^{\xi}\frac{\mathrm{d}\tilde{p}}{\mathrm{d}\xi'}(\xi')\,\mathrm{d}\xi', \quad (11)$$

$$\frac{\mathrm{d}\tilde{p}}{\mathrm{d}\xi}(\xi) = \frac{\mathrm{d}\tilde{p}}{\mathrm{d}\xi}(\xi_0)-k_c^2\int_{\xi_0}^{\xi}F(\xi')\tilde{p}(\xi')\,\mathrm{d}\xi'. \quad (12)$$

This set of equations is well-suited for a numerical resolution by the use of successive approximations. Indeed, the N^{th} order solutions for $\tilde{p}$ and $d_\xi\tilde{p}$ on the left hand-side of equations (11) and (12) can be found by substituting their values at the $(N-1)^{th}$ order in the integral operators on the right hand-side of equations (11) and (12). Introducing the integral operators Ω_1 and Ω_2

$$f \longmapsto \Omega_1(f) = \mathrm{i}k_c\int_{\xi_0}^{\xi}F(\xi')f(\xi')d\xi', \quad (13)$$

$$f \longmapsto \Omega_2(f) = \mathrm{i}k_c\int_{\xi_0}^{\xi}f(\xi')d\xi', \quad (14)$$

the exact solution for $\tilde{p}$ and $d_\xi\tilde{p}$ is finally obtained in the form of an infinite sequence of integral operators

$$\begin{pmatrix} \tilde{p}(\xi) \\ \frac{\mathrm{d}\tilde{p}}{\mathrm{d}\xi}(\xi) \end{pmatrix} = \begin{pmatrix} \sum_{n=0}^{\infty}(\Omega_2\Omega_1)^n & \frac{\Omega_2}{\mathrm{i}k_c}\sum_{n=0}^{\infty}(\Omega_1\Omega_2)^n \\ \mathrm{i}k_c\Omega_1\sum_{n=0}^{\infty}(\Omega_2\Omega_1)^n & \sum_{n=0}^{\infty}(\Omega_1\Omega_2)^n \end{pmatrix} \cdot \begin{pmatrix} \tilde{p}(\xi_0) \\ \frac{\mathrm{d}\tilde{p}}{\mathrm{d}\xi}(\xi_0) \end{pmatrix}, \quad (15)$$

where for instance $(\Omega_2\Omega_1)^n\tilde{p}(\xi_0)$ means

$$(\Omega_2\Omega_1)^n\tilde{p}(\xi_0) = \underbrace{\Omega_2\Big(\Omega_1\Big(\ldots\Omega_2\Big(\Omega_1}_{n \text{ times}}\big(\tilde{p}(\xi_0)\big)\Big)\Big)\Big). \quad (16)$$

Then, using the Navier-Stokes equation, the acoustic velocity $\tilde{v}(x,r)$ is expressed as a function of acoustic pressure, and integrating over a cross section, the mean axial velocity $\langle\tilde{v}(x)\rangle_r$ (where $\langle\,\rangle_r$ denotes the average over a cross section) is expressed as

$$\langle\tilde{v}(x)\rangle_r = \frac{1}{\mathrm{i}k_c Z(x)}\frac{\mathrm{d}\tilde{p}(x)}{\mathrm{d}x}, \quad (17)$$

with

$$Z(x) = \frac{\rho(x)a_c}{1-f_\nu}, \quad (18)$$

$\rho(x)$ being the mean density along the thermoacoustic core. Combining equations (17) and (15) finally gives the acoustic field in the thermoacoustic core as a function of its value at position x_0:

$$\begin{pmatrix} \tilde{p}(x) \\ \langle\tilde{v}(x)\rangle_r \end{pmatrix} = \begin{pmatrix} \sum_{n=0}^{\infty}(\Omega_2\Omega_1)^n & Z(x)\Omega_2\sum_{n=0}^{\infty}(\Omega_1\Omega_2)^n \\ \frac{\xi_x(x)\Omega_1}{Z(x)}\sum_{n=0}^{\infty}(\Omega_2\Omega_1)^n & \frac{Z(x_0)\xi_x(x)}{Z(x)}\sum_{n=0}^{\infty}(\Omega_1\Omega_2)^n \end{pmatrix} \cdot \begin{pmatrix} \tilde{p}(x_0) \\ \langle\tilde{v}(x_0)\rangle_r \end{pmatrix}. \quad (19)$$

Invoking equation (19) yields the transfer matrix of the thermoacoustic core:

$$\begin{pmatrix} \tilde{p}(H_W) \\ \langle\tilde{v}(H_W)\rangle_r \end{pmatrix} = T \times \begin{pmatrix} \tilde{p}(-H_S) \\ \langle\tilde{v}(-H_S)\rangle_r \end{pmatrix} = T_S \times T_W \times \begin{pmatrix} \tilde{p}(-H_S) \\ \langle\tilde{v}(-H_S)\rangle_r \end{pmatrix}, \quad (20)$$

where T_S is obtained using equation (19) with $(x_0,x) = (-H_S,0)$ for a channel radius $D \equiv D_S$ and T_W is obtained using equation (19) with $(x_0,x) = (0,H_W)$ for a channel radius $D \equiv D_W$.

Then, the linear propagation of an harmonic wave in the cold part of the resonator ($H_W \le x \le L - H_S$) can be described by equation (5), taking into account that $T_N \equiv 1$ (and taking $D \equiv D_W$ in equation (4)). The resulting expressions for the counterpropagative components $\tilde{p}^+$ and $\tilde{p}^-$ of acoustic pressure waves in the cold part of the resonator are:

$$\tilde{p}^{\pm}(x) = \tilde{p}^{\pm}(H_W)\mathrm{e}^{\pm\mathrm{i}k_W(x-H_W)}, \quad (21)$$

where the complex wavenumber

$$k_W = k_c\sqrt{\frac{1+(\gamma-1)f_\kappa}{1-f_\nu}} \quad (22)$$

accounts for the thermal and viscous losses in the vicinity of the resonator walls.

Using equations (21) and (17) the mean acoustic velocity $\langle\tilde{v}(x)\rangle_r$ can be expressed as a function of the counterpropagative components $\tilde{p}^+$ and $\tilde{p}^-$ of acoustic pressure $\tilde{p} = \tilde{p}^+ + \tilde{p}^-$ and finally, simple calculations allow us to transform the transfer matrix (equation (20)) into the scattering matrix (equation (1)), and then the coefficient $\mathcal{R}^{\pm}$ and $\mathcal{T}^{\pm}$ are obtained.

2.2. Thermoacoustic amplification coefficient

Now, the method for determining the threshold conditions is laid out. To model the amplification/attenuation of the wave through the thermoacoustic core, a thermoacoustic amplification coefficient α is introduced as follows:

$$\forall x \in [0,L], \quad \tilde{p}_m^{\pm}(x) = \tilde{p}_{m-1}^{\pm}(x)\mathrm{e}^{\alpha}. \quad (23)$$

In this equation, the coefficient α describes the amplitude evolution of counterpropagative waves that travel a closed loop in the system, passing through the thermoacoustic core and then in the waveguide at room temperature T_C.

The sign of α determines whether the acoustic wave is attenuated ($\alpha < 0$) or amplified ($\alpha > 0$) while $\alpha = 0$ corresponds to the threshold condition or to the stationnary regime. Combining equations (1), (21), and (23) gives:

$$\begin{pmatrix} \left(\mathcal{T}^+ - \mathrm{e}^{\alpha-\mathrm{i}k_W L_W}\right) & \mathcal{R}^-\mathrm{e}^{-\mathrm{i}k_W L_W} \\ \mathcal{R}^+\mathrm{e}^{\mathrm{i}k_W L_W} & \left(\mathcal{T}^- - \mathrm{e}^{\alpha-\mathrm{i}k_W L_W}\right) \end{pmatrix} \cdot \begin{pmatrix} \tilde{p}_m^+(H_W) \\ \tilde{p}_m^-(H_W) \end{pmatrix} = \begin{pmatrix} 0 \\ 0 \end{pmatrix}, \quad (24)$$

where $L_W = L - H_S - H_W$ is the length of the waveguide at room temperature. The solution $(\tilde{p}_m^+(H_W), \tilde{p}_m^-(H_W))$ of equation (24) is nonzero if the matrix determinant is zero:

$$\left(\mathrm{e}^{\alpha-ik_W L_W} - \mathcal{T}^+\right) \cdot \left(\mathrm{e}^{\alpha-ik_W L_W} - \mathcal{T}^-\right) - \mathcal{R}^+\mathcal{R}^- = 0. \quad (25)$$

If the temperature distribution in the thermoacoustic core is fixed, a truncated approximate solution for $\mathcal{T}^{\pm}$ and $\mathcal{R}^{\pm}$ can be computed, and introduced in equation (25) to obtain the amplification coefficient α and the corresponding angular frequency ω. Here, we are interested in the most unstable acoustic mode, which is in most cases the first travelling wave mode of the annular waveguide ($f \approx a_c/L$). The quantity $\Delta\phi = \alpha - \mathrm{i}(k_W L_W - 2\pi)$ is introduced, where 2π is in fact the approximate value for $k_W L_W$ in the empty device ($L_W = L$). Substituting $\Delta\phi$ in equation

(25) results in a quadratic equation in $e^{\Delta\phi}$, which admits the solution

$$e^{\Delta\phi} = \Gamma^{\pm} = \left(\frac{\mathcal{T}^{+} + \mathcal{T}^{-}}{2}\right) \pm \sqrt{\left(\frac{\mathcal{T}^{+} - \mathcal{T}^{-}}{2}\right)^{2} + \mathcal{R}^{+}\mathcal{R}^{-}}. \quad (26)$$

Finally, separating equation (26) into real and imaginary parts, the following set of equations is solved:

$$\begin{cases} \alpha^{\pm} = \ln\left|1 + \Gamma^{\pm}(\omega^{\pm})\right| - \Im m\left(k_W(\omega^{\pm})L_W\right) \\ 2\pi = \mathrm{Arg}\left(1 + \Gamma^{\pm}(\omega^{\pm})\right) + \Re e\left(k_W(\omega^{\pm})L_W\right) \end{cases}, \quad (27)$$

If we were interested in the n^{th} travelling wave mode of the device we would only replace 2π by $2n\pi$ in equation (27). As pointed out in equations (26) and (27) there are two possible solutions for α and ω, but it is easy to accept that the physically observable solution is the one which increases in the quickest way. Consequently, the chosen solution $(\alpha, \omega) \in \{(\alpha^-, \omega^-), (\alpha^+, \omega^+)\}$ is that for which

$$\alpha = \mathrm{Sup}(\alpha^+, \alpha^-). \quad (28)$$

2.3. Acoustic field in the whole device

Finally, the acoustic field in the whole device can be computed for some arbitrary temperature distribution, once the corresponding amplification coefficient α and oscillation frequency ω are known. Using equation (21), the acoustic pressure in the cold part of the waveguide is firstly computed as follows:

$$\forall x \in [H_W, L - H_S],$$
$$\tilde{p}(x) = \tilde{p}^{+}(H_W)\left[e^{ik_W(x - H_W)} + \tilde{R}(H_W)e^{-ik_W(x - H_W)}\right], \quad (29)$$

where the complex quantity $\tilde{R}(H_W) = \tilde{p}^{-}(H_W) / \tilde{p}^{+}(H_W)$ is obtained using equation (24):

$$\tilde{R}(H_W) = \frac{e^{\alpha - ik_W L_W} - \mathcal{T}^{+}}{\mathcal{R}^{-}e^{-ik_W L_W}}. \quad (30)$$

Combining equations (29) and (17), the mean acoustic velocity $\langle\tilde{v}(x)\rangle_r$ is also computed.

Then, to obtain the acoustic field in the thermoacoustic core, equation (19) is used. This equation is valid both in the stack region and in the inhomogeneously heated part of the resonator, but each region has to be treated separately, because $Z(x)$, $\xi_x(x)$, Ω_1 and Ω_2 depend notably on the $f_{\nu,\kappa}$ functions which characterize the transverse distribution of oscillating velocity and oscillating entropy in the channel, and which are consequently not the same depending on whether the channel radius D is D_S or D_W.

So, setting the boundary values $\tilde{p}(L - H_S)$ and $\langle\tilde{v}(L - H_S)\rangle_r$ in the right-hand side of equation (19) (i.e. setting x_0 to $L - H_S$), the acoustic field is first computed in the $[-H_S, 0]$ interval. Then, setting the boundary values $\tilde{p}(L)$ and $\langle\tilde{v}(L)\rangle_r$ in the right-hand side of equation (19) (with account of $D \equiv D_W$), the acoustic field is finally computed in the $[L, L + H_W] \equiv [0, H_W]$ interval.

Note that in equation (29), the clockwise pressure wave amplitude $\tilde{p}^{+}(H_W)$, and consequently the amplitudes of acoustic waves are unknown. In fact, to determine the amplitude of the pressure wave at any time in the device, it is necessary to solve the transient problem from the onset of the thermoacoustic instability to the stabilization of the wave amplitude (due to nonlinear processes). Nevertheless, by setting $\tilde{p}^{+}(H_W)$ to an arbitrary value in equation (29), we are able to find the structure of the acoustic field in the whole device, for a given temperature distribution profile $T(x)$. Thus, for all the results presented in the following, $\tilde{p}^{+}(H_W)$ will be set in order to have an input intensity $I(H_W)$ of $1W$, with $I = (1/2)\Re e(\tilde{p}\langle\tilde{v}^{*}\rangle_r)$ (* denoting the complex conjugate), the main object being to understand how and why the amplification coefficient α depends on the details of the temperature distribution $T(x)$.

3. Results

Thermoacoustic energy conversion is known to be controlled notably by the nature of the interaction between the acoustic waves and the solid surfaces. This interaction is characterized by the thicknesses of the viscous and thermal boundary layers δ_ν and δ_κ relative to the channel diameter $2D_S$, where $\delta_\nu = \sqrt{2\nu/\omega}$ and $\delta_\kappa = \sqrt{2\kappa/\omega}$ (ν and κ denoting the dynamic viscosity and thermal diffusivity of fluid, respectively) depend on the temperature $T(x)$ since $\nu \propto \kappa \propto T^{\beta+1}$ (with $\beta = 0.73$ [19]). In our theoretical model, all the geometric properties (stack length, resonator length) and physical properties (stack material, fluid) are adjustable. Here, we will focus only on the role of the temperature distribution when the regime of the acoustic and thermal waves interaction inside the stack varies from the quasi adiabatic (QA) regime ($\delta_{\kappa,\nu}/D_S \ll 1$) to the quasi isothermal (QI) regime ($(\delta_{\kappa,\nu}/D_S)^2 \gg 1$). Thus, the only parameter variations that will be considered here are firstly the temperature distribution $T(x)$, and secondly the thermal conductivity of the fluid at room temperature $K(T_C)$. In fact, the variations of the viscous properties of the fluid are also considered accordingly with $K(T_C)$ variations, because the Prandtl number will be fixed to its value for air ($\sigma = \nu/\kappa = 0.7$). For the remainder of the paper, all the other parameters will be kept constant (except stack length H_S in Figures 14–15). Their values correspond to those of our experimental apparatus [13, 15] as indicated in Table I.

3.1. Transition from the QA regime to the QI regime in the case of the linear temperature distribution

The acoustic field in the whole device is presented in Figure 3 for the case of linear temperature distribution profile at threshold condition ($\alpha = 0$) when the device is filled with air at atmospheric pressure ($\delta_\kappa/D_S = 0.46$). The observed discontinuities for the acoustic velocity at the edges

Table I. Geometrical and physical properties of the model.

Physical properties			
	volumetric mass kg/ m^3	heat capacity J/kg/K	thermal conductivity W/m/K
stainless steel	7900	460	14
stack (cordierite)	2500	900	2.5
fluid (air)	1.2	1003	variable

Geometrical properties	
L	2.24 m
D_W	26.5 mm
stack porosity	0.81
D_S	0.45 mm
H_S	0.15 m
H_W	0.4 m

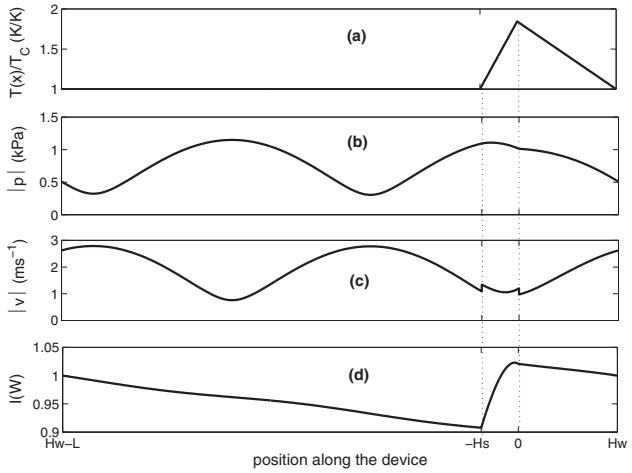

Figure 3. Distribution of the acoustic pressure $|\tilde{p}(x)|$ (b), acoustic velocity $|\tilde{v}(x)|$ (c), and acoustic intensity $I = (1/2)\Re e(\tilde{p}\tilde{v}^*)$ (d) in the whole device, at threshold for the case of the linear temperature distribution profile (a).

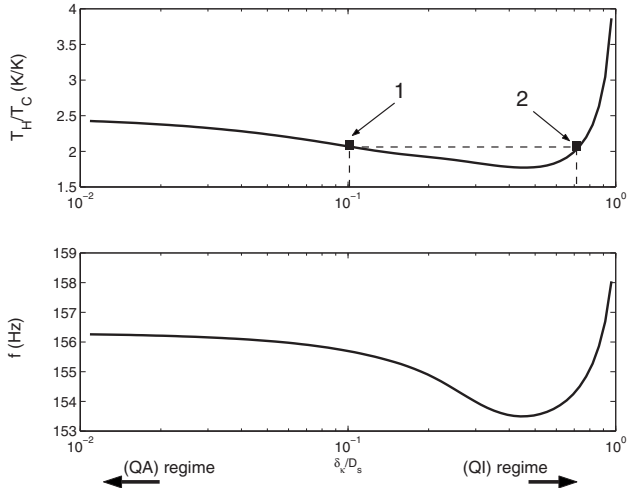

Figure 4. Evolution of the T_H/T_C ratio and frequency f at threshold, versus δ_κ/D_S.

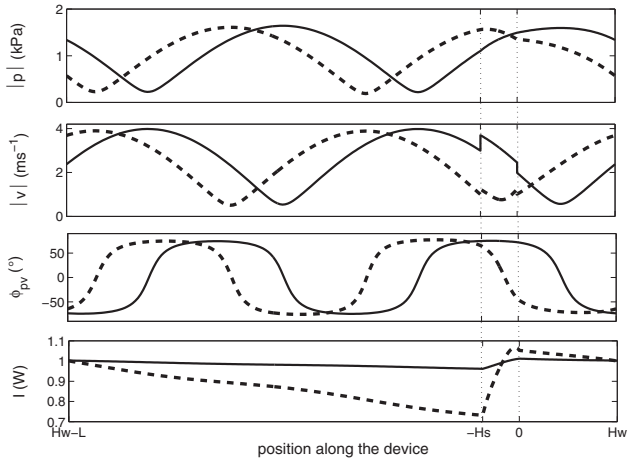

Figure 5. Distribution of the acoustic pressure $|\tilde{p}(x)|$, acoustic velocity $|\tilde{v}(x)|$, phase shift Φ_{pv} and acoustic intensity $I = 1/2\Re e(\tilde{p}\tilde{v}^*)$ in the whole device, at threshold for the case of the linear temperature distribution profile. Solid line: $\delta_\kappa/D_S = 0.1$, dashed line: $\delta_\kappa/D_S = 0.73$.

of the stack are simply due to the flow conservation (with a stack porosity of 0.81). Notice that the acoustic intensity (fig. 3 (d)) produced in the stack exactly compensates for the thermal and viscous losses in the other part of the resonator.

Now, the threshold conditions are analyzed when $\delta_{\kappa,\nu}$ varies (D_S remaining constant) from the quasi adiabatic regime to the quasi isothermal regime. Figure 4 presents the evolution of both hot to cold temperature ratio $T_H/T_C = T(x = 0)/T(x = -H_S)$ and frequency $f = \omega/2\pi$ at threshold as a function of δ_κ/D_S.

The results obtained match earlier experimental results obtained by Yazaki [1]. In particular, they show the existence of a minimum in the threshold temperature ratio at $\delta_\kappa/D_S \approx 0.5$ (i.e. between QA and QI regime). A drastic increase in T_H/T_C is also observable when δ_κ/D_S tends to 1 (QI regime). The threshold frequency f does not change significantly: its order of magnitude remains $f \approx a_c/L$, with small variations predominantly due to temperature dependence of sound velocity a_c in the thermoacoustic core (and perhaps also due to changes in the sound reflexion at the edges of the stack).

In Figure 4, two particular points (referred as 1 and 2) are marked on the threshold curve. For these two points, the threshold condition occurs for the same T_H/T_C, but for different values of $\delta_{\kappa,\nu}/D_S$. Figure 5 presents the acoustic field in the whole device for these two particular points. Although the threshold conditions are the same, it appears clearly that the acoustic pressure $|\tilde{p}|$, acoustic velocity $|\tilde{v}|$, and phase shift Φ_{pv} between $\tilde{p}$ and $\tilde{v}$ are not distributed in the same way in these two particular cases. More particularly, when $\delta_{\kappa,\nu}/D_S$ varies, the pressure and velocity minima/maxima are shifted, and the phase shift also varies. Moreover, the distribution of the acoustic intensity I shows that thermal and viscous losses in the res-

onator are higher for $\delta_\kappa/D_S = 0.7$ (QI regime) than for $\delta_\kappa/D_S = 0.1$ (QA regime).

For a better understanding, these results are analyzed in terms of energy conversion. According to Tominaga [20, equations (105)-(108)], the energy conversion per unit volume due to the thermoacoustic interaction in a single pore of given geometry is written as the sum of four terms, in the frequency domain for an ideal gas:

$$w = w_\kappa + w_\nu + w_{SW} + w_{TW}, \tag{31}$$

where

$$w_\kappa \equiv \frac{1}{2}\frac{\gamma-1}{\rho a_c^2}\Im m(F_S f_\kappa)\omega\,|\tilde{p}|^2 \tag{32}$$

and

$$w_\nu \equiv \frac{1}{2}\omega\rho\frac{\Im m(f_\nu)}{|1-f_\nu|^2}\,|\langle\tilde{v}\rangle_r|^2, \tag{33}$$

are negative quantities which express viscous and thermal losses in the vicinity of the channel walls, respectively.

$$w_{SW} \equiv -\frac{1}{2}\frac{d_x T}{T}\Im m(F_S h)\big|\tilde{p}\big|\big|\langle\tilde{v}\rangle_r\big|\sin(\Phi_{pv}) \tag{34}$$

and

$$w_{TW} \equiv \frac{1}{2}\frac{d_x T}{T}\Re e(F_S h)\big|\tilde{p}\big|\big|\langle\tilde{v}\rangle_r\big|\cos(\Phi_{pv}), \tag{35}$$

proportional to $\sin\phi_{pv}$ and $\cos\phi_{pv}$, represent the standing and travelling wave components of the energy conversion respectively (for a pure travelling wave, $\Phi_{pv} = 0 \Rightarrow w_{SW} = 0$). Here, the functions $f_{\kappa,\nu}$ are given by equations (3)-(4) with $D \equiv D_S$ in equation (4), and the terms F_S and h are expressed as a function of f_κ and f_ν as follows:

$$F_S = \frac{1}{1+ef_\kappa}, \tag{36}$$

$$h = \frac{f_\kappa - f_\nu}{(1-\sigma)(1-f_\nu)}, \tag{37}$$

where $e = C_f/C_s$ is the ratio of heat capacity of the fluid to that of the solid wall.

Finally, the energy conversion terms due to the thermoacoustic interaction in a single cylindrical pore of inner radius D_S and length H_S are derived as follows:

$$W_{\kappa,\nu,TW,SW} = \pi D_S^2 \int_{-H_S}^{0} w_{\kappa,\nu,TW,SW}(x)\,\mathrm{d}x. \tag{38}$$

The total energy conversion in the stack

$$W_{tot} = n_C(W_\kappa + W_\nu + W_{TW} + W_{SW})$$

(where n_C denotes the total number of stack channels) is actually linked to the amplification coefficient α. Indeed, when W_{tot} is equal to the thermal and viscous losses outside the stack, α necessarily vanishes.

In Figure 6, the energy conversion terms are plotted as a function of δ_κ/D_S in transition from the QA regime to the QI regime at threshold conditions. Firstly, the total energy conversion in the stack channel $W = W_\kappa + W_\nu + W_{TW} + W_{SW}$ increases when the regime changes from QA to QI. This can be explained by the fact that when $\delta_{\kappa,\nu}$ increases, the thermal and viscous losses in the resonator also increase, and consequently, the total energy conversion in the stack must also increase in order to satisfy the threshold condition. Secondly, each of the $W_{\kappa,\nu,TW,SW}$ terms varies significantly with $\delta_{\kappa,\nu}/D_S$. In the QA regime, the most important part of the produced work is W_{SW}. In the QI regime, W_{TW} predominates while losses in the stack are primarily due to viscous effects.

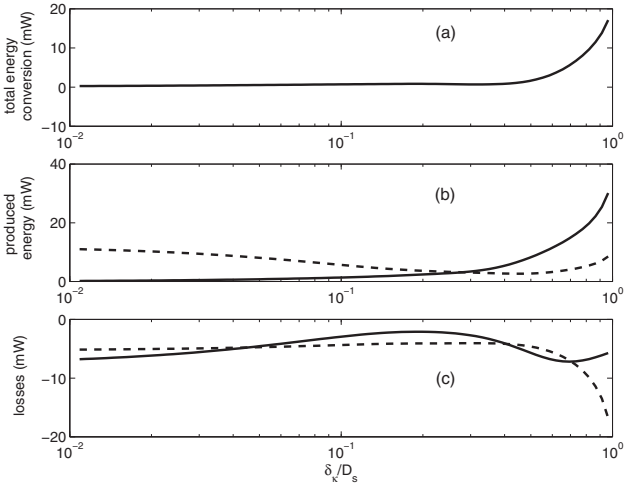

Figure 6. Energy conversion in one stack channel versus δ_κ/D_S at threshold condition ($\alpha = 0$). (a) Total energy conversion. (b) Standing wave component W_{SW} (dashed line) and travelling wave component W_{TW} (solid line) of the produced energy. (c) Viscous component W_ν (dashed line) and thermal component W_κ (solid line) of the losses.

3.2. The role of the temperature distribution in the thermoacoustic core

This section aims at analyzing the effect of the temperature distribution profile when the temperature ratio T_H/T_C and the parameter $\delta_{\kappa,\nu}/D_S$ are fixed. First of all, the thermal and viscous boundary layers $\delta_{\kappa,\nu}$ are set in order to satisfy the condition $\delta_\kappa/D_S = 0.46$ at room temperature (with a fixed Prandtl number $\sigma = \nu/\kappa = 0.7$) . This value corresponds to the experimental conditions of our device [13, 15] when it is filled with air at atmospheric pressure. Then, the hot and cold temperatures T_H and T_C are fixed to satisfy the threshold condition ($\alpha = 0$) for the case of the linear temperature distribution profile. In order to describe different examples of temperature profile in the stack and in the inhomogeneously heated part of the resonator ($-H_S \le x \le 0$ and $0 \le x \le H_W$ domains), the temperatures $T(x = -H_S/2)$ and $T(x = H_W/2)$ are set to several chosen values (control parameters, see Figure 7). By fixing T_H, T_C, and the two control parameters $T(-H_S/2)$ and $T(H_W/2)$, the temperature distribution throughout the thermoacoustic core is then calculated using a cubic spline data interpolation. The normalized tem-

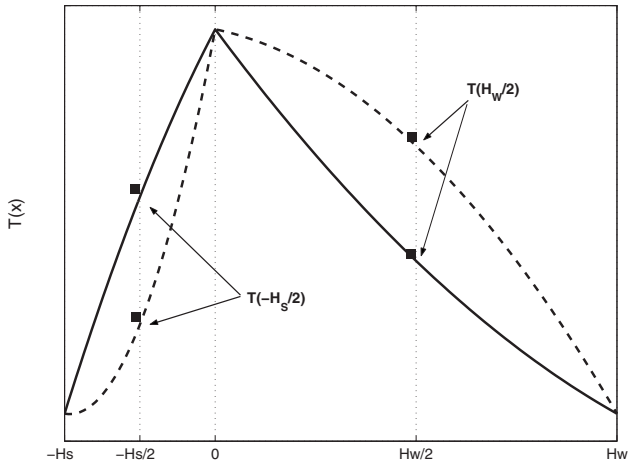

Figure 7. Some temperature distribution profile in the thermoacoustic core. The choice of $T(H_W/2)$ and $T(-H_S/2)$ allows us to describe various physically realistic temperature distributions using a cubic spline data interpolation.

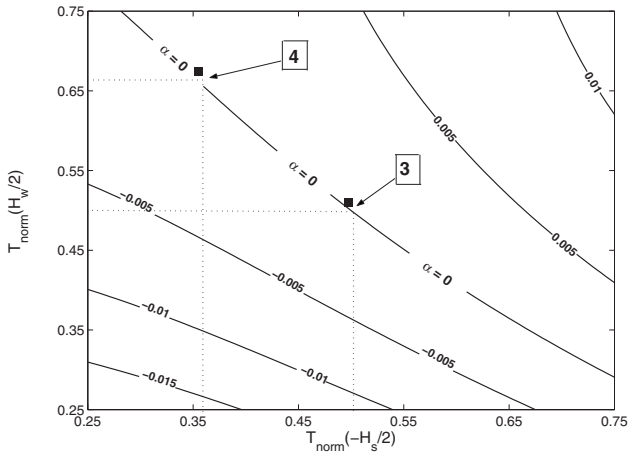

Figure 8. Contour plot of the amplification coefficient α versus $T_{norm}(H_W/2)$ and $T_{norm}(-H_S/2)$, with $H_S = 0.15\,\mathrm{m}$ and $H_W = 0.4\,\mathrm{m}$.

perature T_{norm} at a given position x is also defined as follows:

$$T_{norm}(x) = \frac{T(x) - T_C}{T_H - T_C}. \tag{39}$$

In Figure 8, the evolution of the amplification coefficient α is plotted versus $T_{norm}(-H_S/2)$ and $T_{norm}(H_W/2)$, when H_S and H_W are set respectively to 0.15 m and 0.4 m. The magnitude of the variations of α (which are due only to the temperature distribution profile modification for a fixed T_H/T_C) are $\pm 10^{-2}$. Such variations are significant, because an estimate shows that the amplification of $\alpha = 10^{-2}$ corresponds to an increase in $|\tilde{p}|$ of about 450% within 1 second.

Furthermore, from Figure 8, it follows that the amplification depends not only on the temperature distribution in the stack region ($T_{norm}(-H_S/2)$ parameter) but also closely on the parameter $T_{norm}(H_W/2)$ controlling the temperature distribution profile in the "passive" region $0 \leq x \leq H_W$.

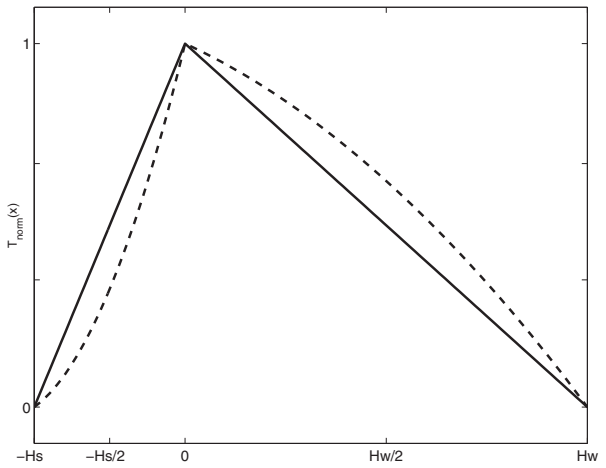

Figure 9. Corresponding temperature distributions for points 3 (solid line) and 4 (dashed line) in Figure 8.
Solid line: $(T_N(H_W/2), T_N(-H_S/2)) = (0.5, 0.5)$,
dashed line: $(T_N(H_W/2), T_N(-H_S/2)) = (0.35, 0.67)$.

In our opinion, the results illustrated in Figure 8 are of primary importance. We suspect these results to be a key to the interpretation of many experimental observations. Particularly, in a previous experimental study of the transient regime [15], we found that the onset of the thermoacoustic instability could give rise to what we called the double threshold effect. During this transient operation, the initial exponential growth of oscillations (first threshold) is followed by a quasi-stabilization (with wave amplitude slowly growing in time), which before the final stabilization is followed by another exponential growth (second threshold), without significant changes of the ratio T_H/T_C. As illustrated in Figure 8, various temperature distributions with the same T_H/T_C correspond to the threshold condition ($\alpha = 0$). Two particular points, referred to as 3 and 4, are marked on the threshold curve in Figure 8. The corresponding temperature distributions for these two particular points are plotted in Figure 9. The first, referred to as 3 in Figure 8, corresponds to the linear temperature distribution profile. The shape of the second temperature profile in Figure 9 (corresponding to point 4 on the threshold curve in Figure 8) suggests the existence of a nonzero directional mass flow (in the $+x$ direction). Such a temperature distribution profile is physically realistic since it could be induced by the directional acoustic streaming [5, 11, 13]. For example, temperature distributions displayed in Figure 9 could be respectively the initial and final states of the temperature field in the transient regime of the prime mover operation. Since the development of the acoustically induced variations of the temperature distribution profile might proceed with a different time scale than the characteristic time of wave amplification, the system, in the process of its transient evolution, may well cross the threshold curve in Figure 8 (between the initial and final state) one or many times. In particular, we suspect the observed double threshold phenomenon [15] to be a consequence of the streaming induced evolution of the temperature distribution in the transient regime

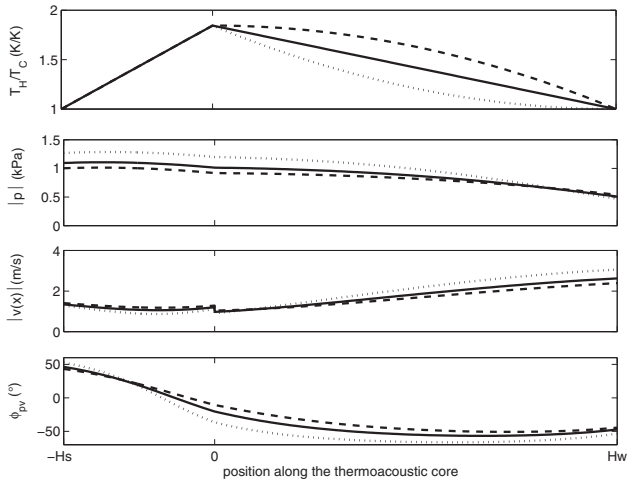

Figure 10. Distribution of the acoustic field in the thermoacoustic core for various temperature distributions in the region $0 \leq x \leq H_W$. Solid line: ($T_{norm}(H_W/2) = 1/2$), $\alpha = 0$; dotted line: $T_{norm}(H_W/2) = 1/4$, $\alpha = -1.1\,10^{-2}$; dashed line: $T_{norm}(H_W/2) = 3/4$, $\alpha = 4.7\,10^{-3}$.

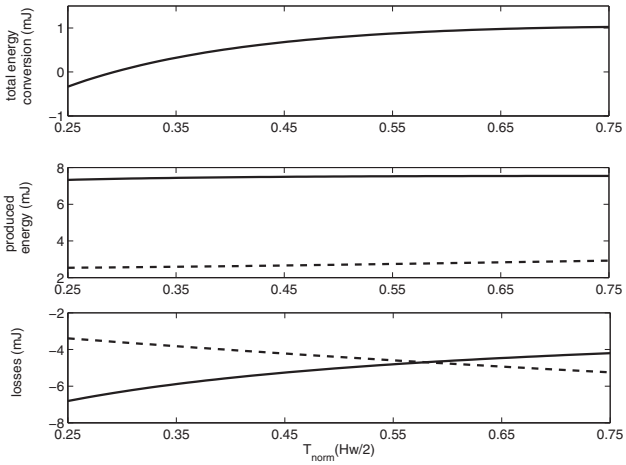

Figure 11. The energy conversion in one stack channel versus $T_{norm}(H_W/2)$. (a) Total energy conversion. (b) Standing wave component W_{SW} (dashed line) and travelling wave component W_{TW} (solid line) of the produced energy. (c) Viscous component W_ν (dashed line) and thermal component W_κ (solid line) of the losses.

of the prime mover operation, which causes the system to cross the threshold curve once between the points 3 and 4. More generally, the results illustrated in Figure 8 suggest that the temperature distribution variations (induced by acoustic streaming or acoustically induced thermal conductivity) throughout the whole thermoacoustic core are a source of multistability for our device, even for a fixed T_H/T_C ratio.

At this stage, we still have no formal explanation concerning the physical reasons of the observed influence of the temperature profile on the thermoacoustic amplification. Therefore, the roles of the stack and of the inhomogeneously heated part of the resonator will be investigated separately. In Figure 10, the evolution of the acoustic field represented by $|\tilde{p}|$, $|\tilde{v}|$, and Φ_{pv} is plotted for different temperature distributions in the inhomogeneously heated part of the resonator. As $T_{norm}(H_W/2)$ increases, the values for $|\tilde{p}|$, $|\tilde{v}|$, and Φ_{pv} in the stack change significantly. Consequently, as shown in Figure 11, the energy conversion terms (equations 32–35) vary.

Here, notice that when $T_{norm}(H_W/2)$ varies, the predominant parameters responsible for the $W_{\kappa,\nu,TW,SW}$ variations are $|\tilde{p}|$, $|\tilde{v}|$, and Φ_{pv}. Indeed, since the temperature field remains constant in the stack, the functions f_κ and f_ν (and consequently F_S and h) only depend on the oscillation frequency $f = \omega/2\pi$, which in fact does not vary significantly with $T_{norm}(H_W/2)$. As a consequence, the energy conversion terms can be written as follows:

$$W_\kappa \propto \int |\tilde{p}|^2 \,\mathrm{d}x, \tag{40}$$

$$W_\nu \propto \int |\tilde{v}|^2 \,\mathrm{d}x, \tag{41}$$

$$W_{SW} \propto \int |\tilde{p}||\tilde{v}| sin\Phi_{pv} \,\mathrm{d}x, \tag{42}$$

$$W_{TW} \propto \int |\tilde{p}||\tilde{v}| cos\Phi_{pv} \,\mathrm{d}x. \tag{43}$$

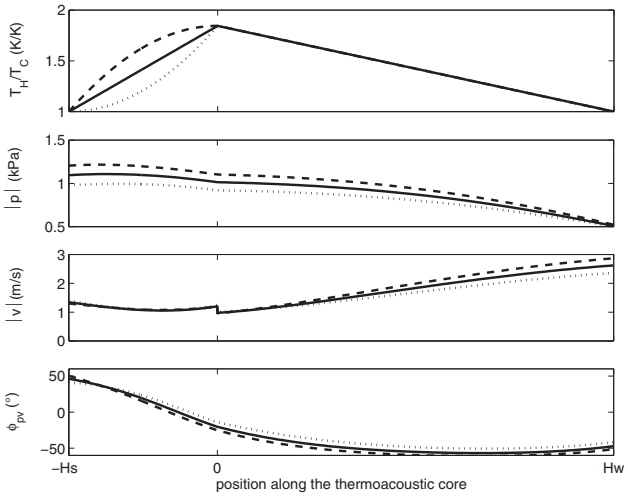

Figure 12. Distribution of the acoustic field in the thermoacoustic core for various temperature distributions in the stack region. Solid line: ($T_{norm}(H_W/2) = 1/2$), $\alpha = 0$; dotted line: $T_{norm}(-H_S/2) = 1/4$, $\alpha = -6\,10^{-3}$; dashed line: $T_{norm}(-H_S/2) = 3/4$, $\alpha = 7\,10^{-3}$.

From the results presented in Figure 11, it follows that the evolution of $|\tilde{p}|$ and $|\tilde{v}|$ in the stack region results in significant variations of W_κ and W_ν, while the produced acoustic energy $W_{TW} + W_{SW}$ remains almost constant. Consequently, the global increase of the total energy conversion W (and consequently of α) as $T_{norm}(H_W/2)$ grows is mostly due to a global decrease of $|W_\kappa + W_\nu|$.

In Figures 12 and 13, the effect of the temperature distribution in the stack is analyzed. Similar to the case when $T_{norm}(H_W/2)$ varies, the $T_{norm}(-H_S/2)$ variations result in changes in the acoustic field distribution (Figure 12). The corresponding evolution of the energy conversion terms is plotted in Figure 13. The simultaneous analysis of Figures 12 and 13 suggests that variations

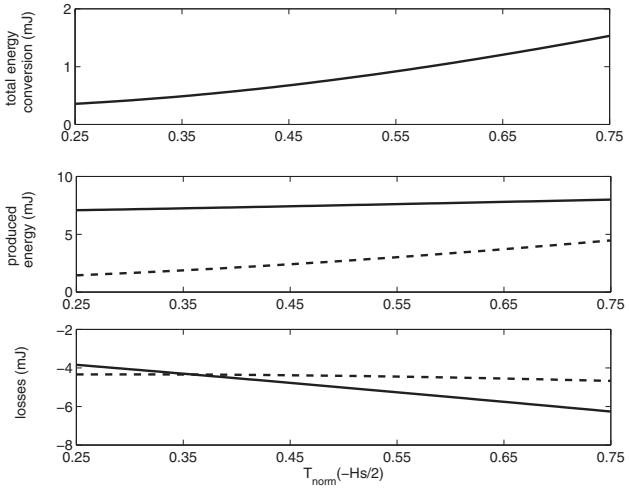

Figure 13. The energy conversion in one stack channel versus $T_{norm}(-H_S/2)$. (a) Total energy conversion. (b) Standing wave component W_{SW} (dashed line) and travelling wave component W_{TW} (solid line) of the produced energy. (c) Viscous component W_ν (dashed line) and thermal component W_κ (solid line) of the losses.

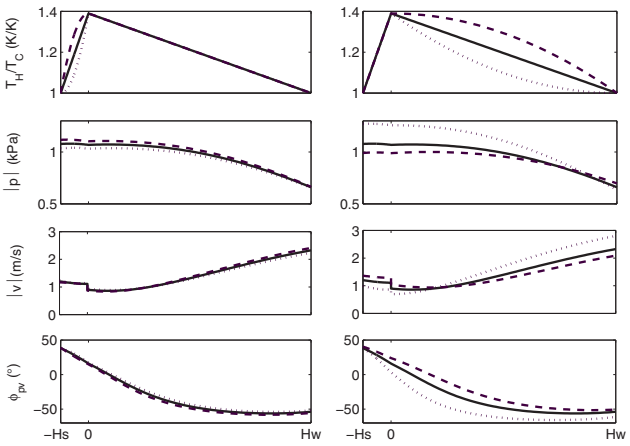

Figure 14. Distribution of the acoustic field in the thermoacoustic core for various temperature distributions , with $H_S = 0.05\,\mathrm{m}$ and $H_W = 0.4\,\mathrm{m}$.

in the thermoacoustic amplification are mostly due to variations of $|\tilde{p}|$ and Φ_{pv} in the stack (and as a consequence, of W_κ, W_{TW}, and W_{SW}). Nevertheless, the relationship between energy conversion and acoustic variables is more complex than in equation (40) when the temperature profile in the stack changes. For instance, the influence of the changes in f_κ and f_ν due to temperature dependence of κ and ν should be taken into account.

At this stage of the paper, it must be remembered that H_S and H_W were chosen in accordance with our experimental device. In Figures 14 and 15, the effect of the temperature distribution profile is analyzed when the stack length H_S is shortened to $0.05\,\mathrm{m}$. In this particular case, as illustrated in Figure 14, the effect of the temperature distribution in the stack does not result in significant changes of the acoustic field while it is not the case when $T_{norm}(H_W/2)$ varies. In the same way, as illustrated in

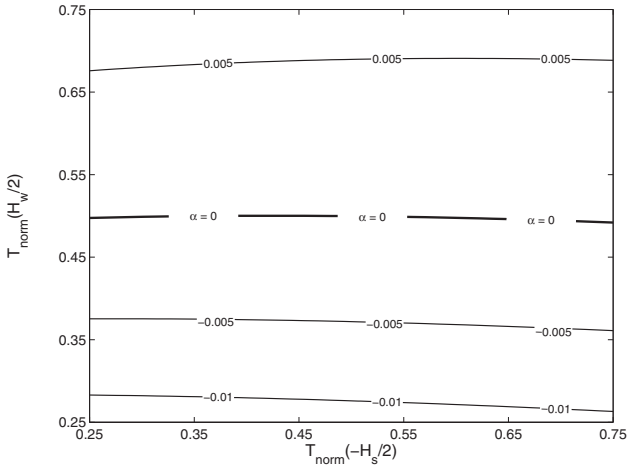

Figure 15. Contour plot of the amplification coefficient α versus $T_{norm}(H_W/2)$ and $T_{norm}(-H_S/2)$, with $H_S = 0.05\,\mathrm{m}$ and $H_W = 0.4\,\mathrm{m}$.

Figure 15, the variations of α are clearly more sensitive to the temperature distribution in the region $0 \leq x \leq H_W$ than to the one in the stack.

Consequently, the influence of the temperature distribution on the thermoacoustic amplification process in an annular thermoacoustic prime mover is mostly due to the influence of the temperature field on the structure of the acoustic field. In particular, the passive temperature distribution in the region $0 \leq x \leq H_W$ acts basically as a mixer of counterpropagating acoustic waves. Both amplitudes and phases of the waves reflected (or transmitted) through this layer depend not only on T_H/T_C but also strongly on the $T(x)$ profile.

4. Conclusion

In this paper, an analytical model is presented, allowing the computation of the acoustic field in an annular thermoacoustic prime mover, for any temperature field in the thermoacoustic core, without restriction on the stack length. The influence of the temperature distribution profile (i.e. linear or not) is investigated. An important result is that the temperature distribution throughout the whole thermoacoustic core (including the inhomogeneously heated part of the resonator) has an important effect on the thermoacoustic amplification. It is demonstrated that changing the temperature field results in variations of the acoustic variables $|\tilde{p}|, |\tilde{v}|$, and Φ_{pv} in the stack region, and consequently in variation of the produced acoustic work. It may be of primary importance when studying the transient regime of the prime mover operation. Indeed, the heat transfer due to acoustically enhanced thermal conductivity and acoustic streaming may change the shape of the temperature field (and also diminish the T_H/T_C ratio) during the process of wave amplification. Those acoustically induced variations of the temperature distribution may proceed with a different time scale than the characteristic time of wave amplification, giving

rise to complicated dynamical behaviours. Particularly, we suspect that the streaming induced evolution of the temperature field in the transient regime may explain the earlier observed double-threshold phenomenon. A numerical investigation of the transient regime is now in progress, where the heat transfer equation is coupled to the acoustic problem by taking into account the forced convection due to acoustic streaming and the acoustically induced thermal conductivity. The objective of the investigation is to qualitatively reproduce the experimental results, in order to relate the parameters controlling transient interactions between acoustic and temperature fields to the measurable parameters of the experimental thermoacoustic devices.

Acknowledgement

This work was supported by the Direction Générale de l'Armement (D.G.A.) under contract $n^{o}99-34072/DSP$.

References

[1] T. Yazaki, A. Iwata, A. Meakawa, A. Tominaga: Traveling wave thermoacoustic engine in a looped tube. Phys. Rev. Let. **81** (1998) 3128–3131.

[2] S. Backhaus, G. W. Swift: A thermoacoustic stirling heat engine: detailed study. J. Acoust. Soc. Am. **107** (2000) 3148–3166.

[3] P. H. Ceperley: A pistonless stirling engine - the traveling wave heat engine. J. Acoust. Soc. Am. **66** (1979) 1508–1513.

[4] T. Yazaki, A. Tominaga, A. Narahara: Large heat transport due to spontaneous gas oscillation induced in a tube with steep temperature gradients. Journal of Heat Transfer **105** (1983) 889–894.

[5] D. Gedeon: DC gas flows in Stirling and pulse-tube cryocoolers. Cryocoolers **9** (1997) 385.

[6] A. A. Atchley, H. E. Bass, T. J. Hofler: Development of nonlinear waves in a thermoacoustic prime-mover. – In: Frontiers in nonlinear acoustics. M. F. Hamilton, D. T. Blackstock (eds.). 1990, 603.

[7] H. Yuan, S. Karpov, A. A. Prosperetti: Simplified model for linear and nonlinear processes in thermoacoustic prime-movers. Part 2: nonlinear oscillations. J. Acoust. Soc. Am. **102** (1997) 3497–3506.

[8] V. Gusev, H. Baillet, P. Lotton, M. Bruneau: Asymptotic theory of nonlinear acoustic waves in a thermoacoustic prime-mover. Acustica-acta acustica **86** (2000) 25–38.

[9] V. Khokhlova, O. Sapozhnikov, S. Kasheeva, P. Lotton, V. Gusev, S. Job, M. Bruneau: Effects of nonlinear saturation in propagation of acoustic wave with frequency-dependent amplification. Sov. Phys. Izvestia of Russian Academy of Sciences **64** (2001) 2334.

[10] V. A. Muller, E. Lang: Experimente mit thermisch getriebenen Gasflüssigkeitsschwingungen. J. Appl. Math. Phys. (ZAMP) **36** (1985) 358.

[11] V. Gusev, S. Job, H. Baillet, P. Lotton, M. Bruneau: Acoustic streaming in annular thermoacoustic prime-movers. J. Acoust. Soc. Am. **108** (2000) 934–945.

[12] M. Mironov, V. Gusev, Y. Auregan, P. Lotton, M. Bruneau, P. Piatakov: Acoustic streaming related to minor loss phenomenon in differentially heated elements of thermoacoustic devices. J. Acoust. Soc. Am. **112** (2002) 441–445.

[13] S. Job, V. Gusev, P. Lotton, M. Bruneau: Acoustic streaming measurements in annular thermoacoustic engines. J. Acoust. Soc. Am. **113** (2003) 1892–1899.

[14] G. B. Chen, T. Jin: Experimental investigation on the onset and damping behaviour of the oscillation in a thermoacoustic prime-mover. Cryogenics **39** (1999) 843–846.

[15] G. Penelet, E. Gaviot, V. Gusev, P. Lotton, M. Bruneau: Experimental investigation of transient nonlinear phenomena in an annular thermoacoustic prime-mover: observation of a double-threshold effect. Cryogenics **42** (2002) 527–532.

[16] M. F. Hamilton, Y. A. Ilinskii, E. A. Zabolotskaya: Nonlinear two-dimensional model for thermoacoustic engines. J. Acoust. Soc. Am. **111** (2002) 2076–2086.

[17] S. Job: Etudes théoriques et expérimentales d'un générateur thermoacoustique annulaire à ondes progressives. PhD Thesis, Université du Maine, 2001.

[18] G. W. Swift: Thermoacoustic engines. J. Acoust. Soc. Am. **84** (1988) 1145–1180.

[19] N. Rott: Thermoacoustics. Adv. Appl. Mech. **20** (1980) 135–175.

[20] A. Tominaga: Thermodynamic aspects of thermoacoustic theory. Cryogenics **35** (1995) 427–440.